

Mechanics and modelling of high-frequency mechanical impact and its effect on fatigue

Guénaél Le Quilliec · Henri-Paul Lieurade ·
Marc Bousseau · Monssef Drissi-Habti ·
Geneviève Inglebert · Pascal Macquet · Laurent Jubin

Received: 10 January 2011 / Accepted: 6 June 2012 / Published online: 7 December 2012
© International Institute of Welding 2012

Abstract High-frequency mechanical impact is a recent improvement method which is probably one of the most effective for treating welded assemblies. A number of experimental results relating to this process are presented in this article. These results lead to better understand the mechanisms of the process, to outline the influence of the operating parameters and to confirm the role played by the initial quality of treated welds. In addition, a process is proposed in order to numerically estimate the fatigue life improvement reached after treatment. All these results were obtained in the scope of a study whose long-term aim is to propose an approach that can be industrially applicable for fatigue design of welded assemblies treated by high-frequency mechanical impact.

Keywords (IIW Thesaurus) High frequency · Mechanical stress relief · Welding · Fatigue improvement · High strength steels · Indentation · Mechanical properties

1 Introduction

In comparison with the base and filler materials used, welded structures have relatively low fatigue strength. This can be explained by the number of cycles required for a micro-crack to initiate. The initiation stage is often predominant in the fatigue life of metallic materials. It becomes very weak in the specific case of welded assemblies. This is mainly caused by the usual presence of residual tensile stresses, high stress raisers and an often poor surface

Doc. IIW-2322, recommended for publication by Commission XIII "Fatigue of Welded Components and Structures".

G. Le Quilliec (✉)
Cetim of Nantes, IFSTTAR of Nantes,
LISMMA-Supméca
of Paris, Paris, France
e-mail: guenael_le_quilliec@yahoo.fr

H.-P. Lieurade (✉)
Cetim of Senlis, Senlis, France
e-mail: lieuradehp@gmail.com

M. Bousseau
CESMAN-DCNS Research, Indret, France
e-mail: marc.bousseau@orange.fr

M. Drissi-Habti
IFSTTAR of Nantes, Nantes, France
e-mail: monssef.drissi-habti@ifsttar.fr

G. Inglebert
LISMMA-Supméca of Paris, Paris, France
e-mail: genevieve.inglebert@supmeca.fr

P. Macquet · L. Jubin
Cetim of Nantes, Nantes, France

P. Macquet
e-mail: pascal.macquet@expert-meca.fr

L. Jubin
e-mail: laurent.jubin@cetim.fr

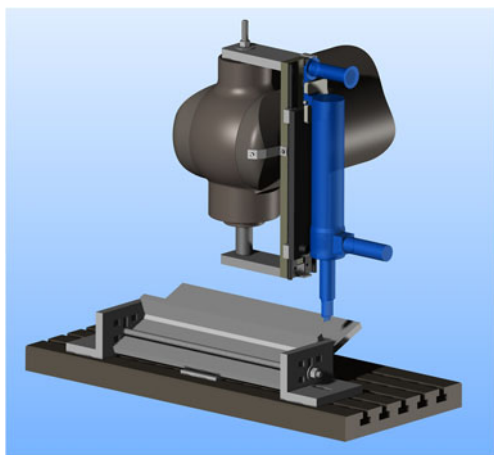
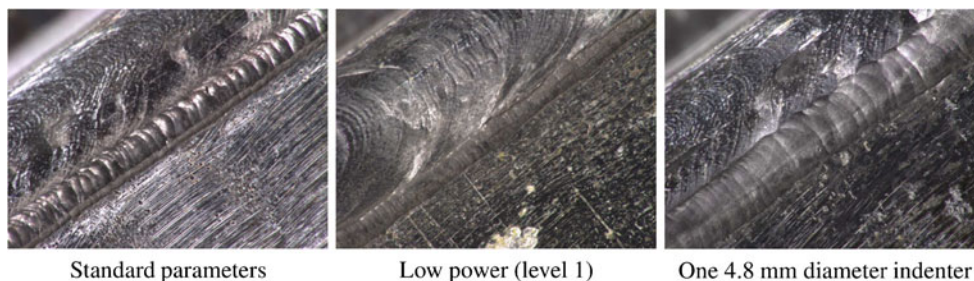


Fig. 1 Semi-automatic treatment device

roughness at the weld toe. It is therefore essential to have a design that takes into account the specific features in the case of exposure to cyclic loading. In addition, the precise study of the loading that will be undergone by the welded assembly will enable better design of the welded connection and make it possible to justify whether or not post-treatments should be applied such as TIG dressing, grinding, shot peening or hammer peening [1]. These treatments will make possible to increase the fatigue life by mainly increasing the initiation period of fatigue cracks. For a given fatigue life, they permit to save weight due to the fatigue strength increase. The gain will be all the more significant since the stresses will be limited and ultimate tensile strength will be high [2].

One of the most recent (and probably one of the most efficient) improvement methods is high-frequency mechanical impact or HFMI (e.g. [3–6]). With respect to conventional hammer peening, HFMI stands out thanks to its improved simplicity and user comfort. Applying this treatment has been shown to be very competitive making the most of the advantages provided by certain materials in the field of welding and more particularly high-strength steels [7]. However, there are a certain number of technical difficulties that must be overcome to apply HFMI whether for new or old structures. Using the various results available for this process is uneasy for the fatigue design of an HFMI-treated welded assembly for a given configuration and

Fig. 2 Change of the hammered groove on the welded assembly for the various treatment parameters



Standard parameters

Low power (level 1)

One 4.8 mm diameter indenter

treatment parameters. Such an approach have been recently proposed by Yildirim and Marquis [8], based on a statistical analysis of experimental results taken from the literature. However, this preliminary solution to predict the rate of improvement does not take into account the material strength yet. Moreover, premature failures are often observed in the literature and the cause of these early failures is not clearly identified.

The work presented in this article falls within the framework of a project which should in the long run propose an industrially applicable approach with the aim of increasing the guaranteed fatigue life of new structures and to extend the one of existing structures.

2 Experimental analyses of the effects of high-frequency mechanical impact

2.1 Configuration of the welded assembly

Cruciform non-carrying-fillet welded joints are one of the most common structural details of welded structures as well as the most susceptible to fatigue phenomenon. This assembly configuration was therefore selected for the HFMI study in S355K2-grade rolled structural steel, 15 mm thick, with a flux-cored-type filler metal which has a similar grade (T42 4 MC 2H5). All the assemblies were performed with the automatic MAG process which makes it possible to ensure a good quality as well as proper repeatability of the operation on each run. The welding operation was carried out in flat position which results in run profiles that have a higher quality with regard to fatigue strength. Finally, the quality of the welded was controlled using a laser triangulation to assure the higher weld quality.

2.2 HFMI treatment equipment

The Esonix-type Ultrasonic Impact Treatment device was selected to perform high-frequency mechanical impact treatments. This choice was mainly motivated by the many results given in the literature relating to this hammer model. Comparisons may be made at the end of the treatment.

Table 1 Transverse (1 to 4) and longitudinal (5 to 7) roughness measurements in the groove of a weld toe hammered with the standard parameters

	No. 1	No. 2	No. 3	No. 4	No. 5	No. 6	No. 7
R_t [μm]	1.7	1.9	1.6	3.7	18.5	13.7	14.4

The tool is powered and controlled by an alternating current generator (Esonix PLC05 type). A water cooling device is used to limit transducer heating during the treatment. The generator has five power levels which vary the amplitude of the sonotrode vibrations. Whatever is the level of power selected, the excitation frequency remains equal to the resonance frequency of the transducer that is 27 kHz for the model used.

At the end of the tool, a set of indenters crosses a rubber strip inserted in the removable support in order to keep the indenters in their casing when the tool is inactive. Indenters with 3 mm in diameter are recommended for the treatment of steel welded assemblies. The measurements carried out on them indicated that the rounded edge has a main radius of approximately 2.4 mm and a secondary blend radius of approximately 0.86 mm.

The transducer, sonotrode and indenter assembly (mechanical impact device) are suspended in the casing in order to isolate the operator from residual vibrations. The suspension spring is pre-stressed upon assembly so that there needs to be a certain pressure for the mechanical impact system to be released from stop position during the treatment. Depending on the position of the tool, its weight acts in addition to the pressure applied by the operator. The mean contact force of the indenters on the treated surface was measured for the following three directions:

- In vertical position, indenters directed downwards, the force varies between 60 and 70 N depending on whether the spring is close to the lower or upper stop;

Fig. 3 3D surface and depth level (along z), expressed in false colours of the central zone of a groove from a base metal hammered

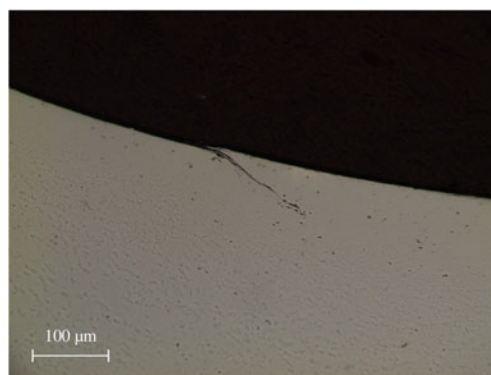
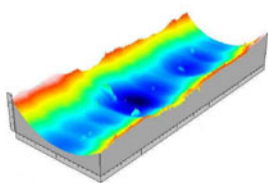


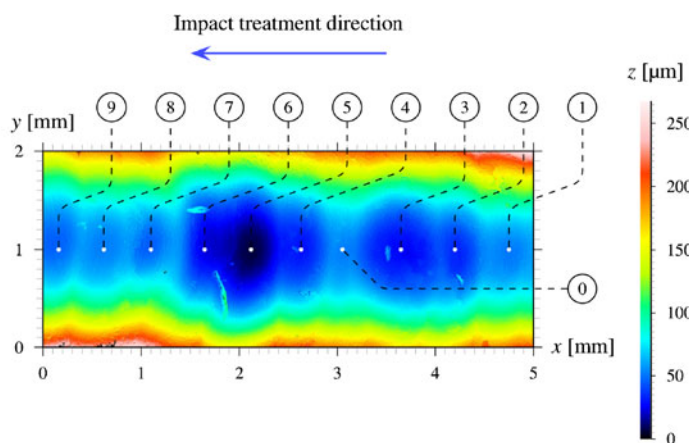
Fig. 4 Fold type defects on the base metal sample treated with standard parameters

- In horizontal position, it varies between 35 and 45 N, and the weight is no longer involved in the process;
- Finally, in vertical position, indenters directed upwards, the weight acts in opposition and the mean contact force only varies between 10 and 20 N.

2.3 Treatment conditions and standard parameters

A specific assembly was adapted on a conventional milling machine in order to best control the treatment parameters (Fig. 1). The tool is assembled vertically above the part to be treated which may be flanged in a sloped position on the moving table. A mobile support guides the hammer in vertical translation with a low stop. Depending on the vertical position of the table, this low stop helps to adjust and constantly maintain the contact force value. In addition to the direction of the tool or the part and the contact force, this assembly helps to simply control the pass speed by taking advantage of the automatic feed system of the milling machine table.

The high-frequency mechanical impact treatment tests were carried out in various configurations. Only one



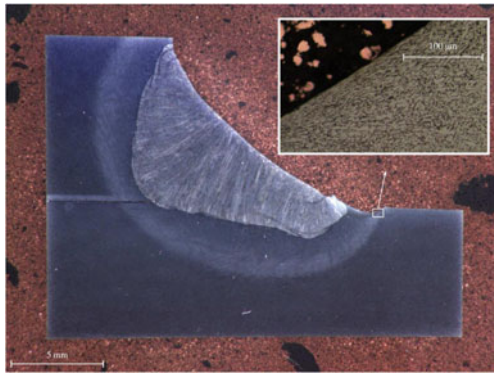


Fig. 5 General microstructure of the weld zone treated with standard parameters and magnification at the impacted surface on base metal side

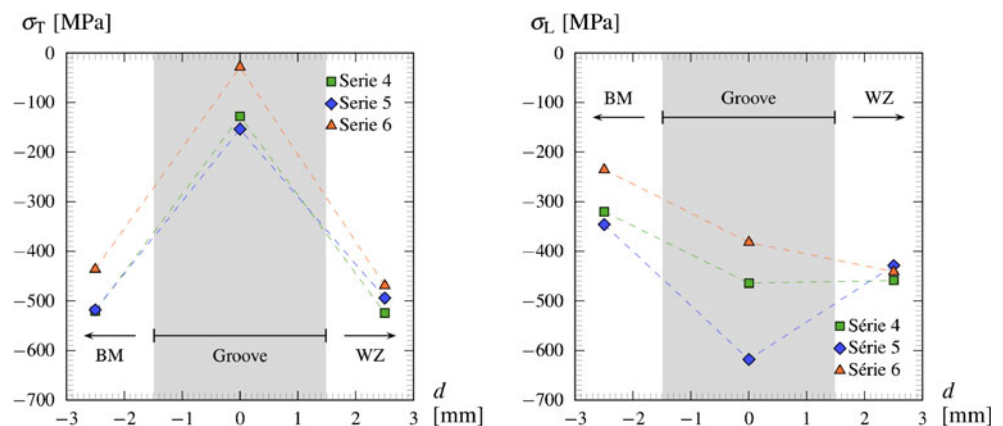
parameter varies at a time with the following standard values for the stationary parameters:

- Vertical position, indenters directed downwards;
- Contact force of the indenters of 70 N;
- Feed rate of 400 mm/min;
- One single pass;
- Maximum power level (5/5, 1,200 W);
- Twenty-three-degree angle between the tool axis and the normal at the assembly main plate;
- Four 3-mm diameter indenters (or three 4.8-mm diameter indenters) aligned in the treatment direction for the tests on the base metal;
- Reduced to only two 3-mm diameter indenters (or one 4.8-mm diameter indenter) for the welded assemblies.

The number of indenters for the treatment of welded assemblies was decreased due to the difficulties experienced in following the profile of the weld toes. There is greater freedom of movement in the vertical direction obtained using only two indenters and no untreated zone was observed.

It is worth noting that the indenters are consumables. The 3-mm diameter indenters were used without lubrication

Fig. 6 Transverse (*left-hand side*) and longitudinal (*right-hand side*) residual stresses with respect to the groove, measured on a cruciform welded joint hammered with the standard parameters



and renewed every metre in order to prevent any failure during treatment. Otherwise, if they are used for an extended period this would cause either their strain for low feed rates stemming from a greater heating (causing a blue stain at the end of the indenters through surface oxidation), or fatigue failure in their housing for higher feed rates.

Finally, ear protection is recommended in order to attenuate the noise generated by the ultrasonic transducer and by the repeated impacts of the indenters between the sonotrode and the surface of the part to be treated. For information, a 96-dBA sound level was recorded at a distance of 50 cm from the edge of the tool during treatment. This level is higher than that expected based on the literature.

2.4 Aspect of the grooves treated

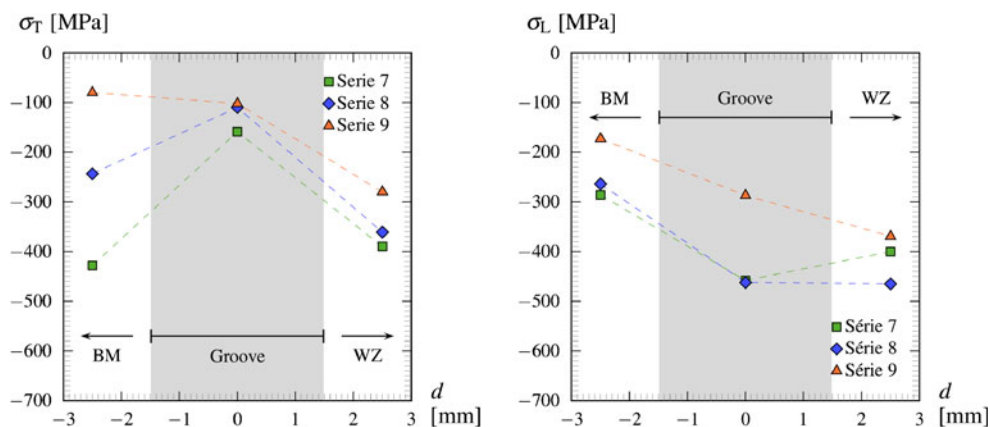
The general aspect of the grooves treated was measured on the cruciform welded assemblies (Fig. 2). Mechanical impact striations systematically appear whatever is the power used. It can also be noted that at low power, the initial weld toe is still present in places. Furthermore, a ‘flaking’-type damage appears on occasions, especially for higher coverage rate (two passes and/or low speed). Finally, it should be noted that the treatment with a 4.8-mm diameter indenters results in a significant improvement of the weld toe radius. However, the treatment depth obtained remains limited in this last case. An excessively closed toe angle may prevent this type of indenters from reaching the weld toe itself.

2.5 Profiles of the grooves and surface roughness

2.5.1 Measurements by mechanical contact

A first series of measurements was carried out by mechanical contact using a ‘Somicronic-Surfscan 35’ profilometer. These measurements were performed on a length varying

Fig. 7 Transverse (left-hand side) and longitudinal (right-hand side) residual stresses with respect to the groove, measured on a cruciform welded joint hammered with standard parameters and fatigue loaded (95,000 cycles at $R=-1$ and $\Delta\sigma=566$ MPa)



from 1.6 to 5 mm based on the accessibility of the probed zone at the rate of one measurement point every 2 μm.

The results obtained reveal that there is a certain uniformity for each of the two measurement directions. From a macroscopic standpoint, it can be noted that the groove radius in the zone with greater stress raiser corresponds more to the blend radius of the indenters than their main tip radius.

On a smaller scale, the roughness deduced is given in Table 1. Maximum roughness height R_t remains generally less than 4 μm in the transverse direction to the groove and ranges between 10 and 20 μm in the collinear direction. These values associated with the blend radius obtained at the weld toe are especially interesting with respect to the fatigue strength of welded assemblies, given the irregularities usually present in this zone.

2.5.2 Optical measurements

• Methodology

An optical measurement analysis was also carried out using a ‘Stil-Micromesure 2’ station. The optical pen selected enables a lateral precision less than 0.1 μm for a vertical precision of a few nanometres. However, the measurement range is limited to 300 μm in depth and a maximum slope of the scanned surface of ±28°. Given that the slope at each edge of the hammered

groove is too steep to be detected by the selected optical pen, the measurement zone was limited to the centre of the groove over a width of 2 mm (width of the groove, 3 mm). The measurement spacing was set to 1 μm in both directions.

The 3D surface obtained on a base metal sample (hammered with the standard parameters) is given in Fig. 3. Impressions 1 to 9 correspond to those of the last of the four indenters which contributed to generate the groove.

• Estimation of the impact frequency

Whereas a constant feed rate was dictated at 400 mm/min for this sample, the impacts generated by the treatment device are visibly not quite periodic. The zone of index 0 separating the third and fourth impacts corresponds moreover to a space that was not hammered by the last of the four indenters.

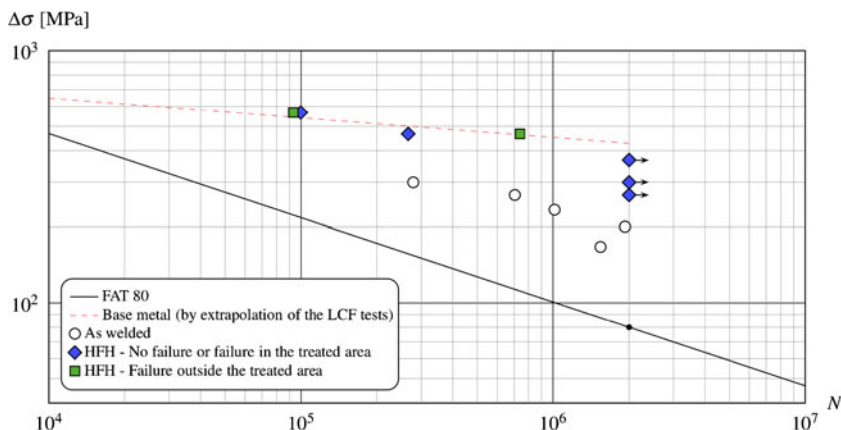
All these impacts make it possible to estimate a mean impact frequency of approximately 48 Hz for the analysed sample by considering:

$$f_m = \frac{N \times v \times n}{l} \tag{1}$$

With:

- N The number of indenters
- n The number of impacts identified

Fig. 8 Fatigue results of the welded joints at $R=-1$ and related estimations



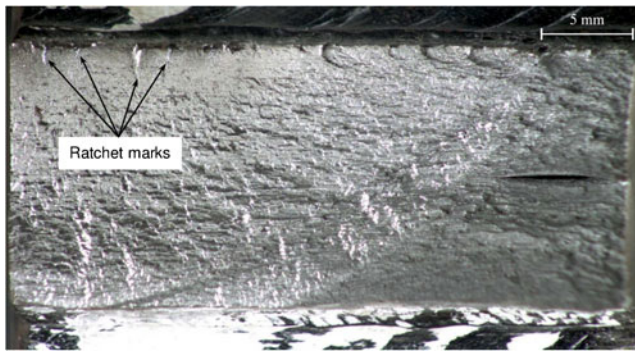


Fig. 9 Fracture surface of a welded assembly treated by HFMI and broken in the hammered zone

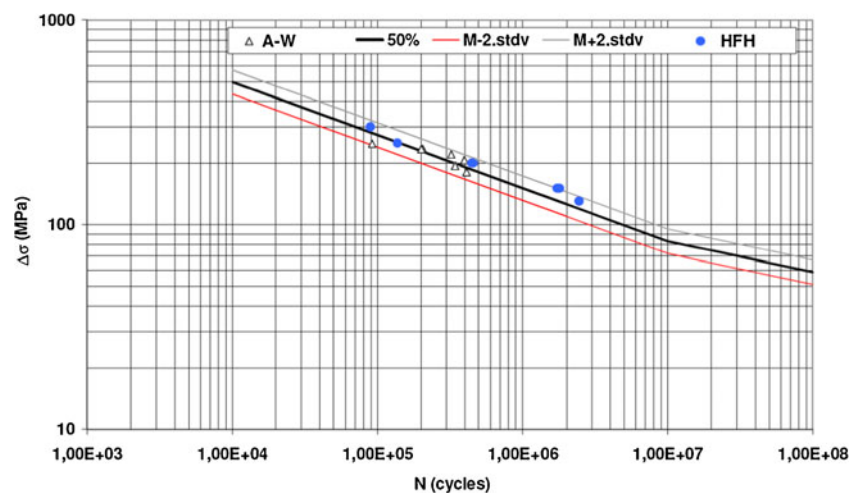
- v The feed rate (in metre per second)
- l The analysed length (in metre)

In the case of the welded assembly treated with the standard parameters and two indenters, an optical microscopic analysis helped to identify a set of 49 impacts over an analysed length of 3 cm (that is, a distance between impacts of approximately 60 μm). By applying the proposed relation (1), we obtained a mean impact frequency of 21.8 Hz (for the two indenters used). This result is similar to that estimated on the base metal (treated with 4 indenters) from Fig. 3 if only the frequency per indenter is considered, that is 12 Hz on the base metal and 10.9 Hz on the welded assembly. These impact frequencies are however markedly less than those given in the literature. For example, the frequency measured by Statnikov et al. [9] range between 200 and 350 Hz for four indenters, that is between 50 and 87.5 Hz per indenter.

2.6 Microstructure and surface defects caused

In addition to the peeling (or flaking) observed on surface for high coverage rates, Fig. 4 reveals the presence of material

Fig. 10 Fatigue results at on cruciform joints composed of DH36 steel at $R=0.1$ [11]



folds which appear more occasionally and essentially for higher treatment powers (levels 4 and 5). Figure 5 gives an example of the microstructure identified in the treated weld toe. As observed in the literature, the grains are moderately elongated in depth and more pronounced on surface. It should be noted that the depth of the groove caused by the tool for the standard parameters is approximately 0.2 mm.

2.7 Residual stresses

X-ray diffraction measurements were carried out using a chrome tube and a linear detector (making it possible to register the radiation of the chrome for the family of lattice planes (211) of phase α of the steel), on two different specimens:

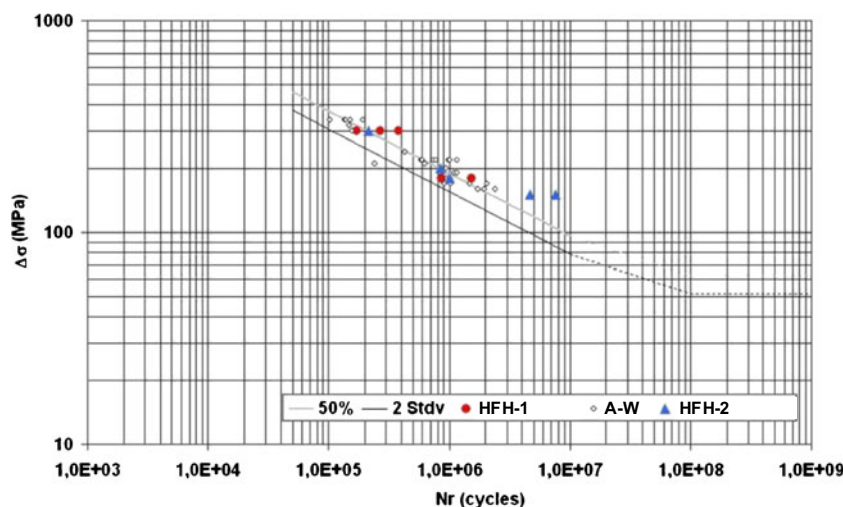
- Welded assemblies treated at the weld toe with standard parameters (Fig. 6);
- Welded assemblies treated then submitted to fatigue loading before the residual stress measurements (Fig. 7).

The collimator used leads to an irradiated volume of 2.5 (longitudinally) \times 1.0 (transversally) \times 0.006 (depth) (in cubic millimetre). The decision was made not to carry out any specific preparation of the groove surface for these measurements except for cleaning with hydrochloric acid. The analyses were carried out along the longitudinal and transverse directions of the groove.

The results, presented in Figs. 6 and 7 are only qualitative given the non-flat geometry of the groove and its surface roughness (striations) which affects the accuracy of the results. However it can be observed that:

- Relatively high compressive stresses are present on the edge of the groove in both directions;
- The longitudinal stresses in the hollow of the groove are strongly compressed (between -300 and -600 MPa) whereas the transverse stresses are subject to low compression;

Fig. 11 Fatigue results at $R=0.1$ on butt-welded joints composed of S690QL steel [12]



- Fatigue loading does not result in significant relaxation of the transverse residual stresses located in the hollow of the groove.

2.8 Fatigue tests

After treatment, the weld test coupons were cut and machined in order to make the fatigue test specimens. Reverse tensile tests ($R=-1$) were carried out on the as-welded cruciform welded assemblies or after HFMI treatment. Figure 8 highlights the satisfactory fatigue strength of the as-welded assembly, in compliance with the previously mentioned welding quality, as well as the remarkable increase of fatigue life in the case of the treated assemblies, especially for long lives.

On the same figure, the base metal fatigue curve at 50 % of failure probability, estimated by extrapolation of the low cycle fatigue curve, was presented in red dotted line. In theory, this curve represents the optimum fatigue strength which may be reached by the treated welded assemblies. As a matter of fact, if treatment gives rise to greater fatigue strength of the hammered zone than that of the base metal, the latter becomes the dimensioning element of the assembly.

The stress ratio $R=-1$ results in a cyclic contact of the crack surfaces which restricts analysis. However on Fig. 9, several ratchet marks can be seen around the hammered surface. These radial marks are due to multiple initiations and joining of micro cracks in the hollow of the groove caused by the treatment.

For the specimens broken outside of the hammered zone, a single initiation point was noted. This initiation point is located far from the weld toe.

2.9 Experimental study of the influence of operative parameters

Some additional tests have been carried out to study the influence of initial weld quality and tool direction.

2.9.1 Initial weld quality influence

The influence of initial weld quality was studied on DH36¹ cruciform welded assemblies with a convex weld shape. It can be noted on Fig. 10 that the improved fatigue strength of the treated assemblies (blue points) is not significant in comparison to the results obtained on the as-welded assemblies (black triangles). This low improvement is explained by the relatively low connecting angle at weld toe induced by the convex shape of the weld, leading to fold defects. These results confirm the ones given in the literature (e.g. [10]).

2.9.2 Tool direction influence

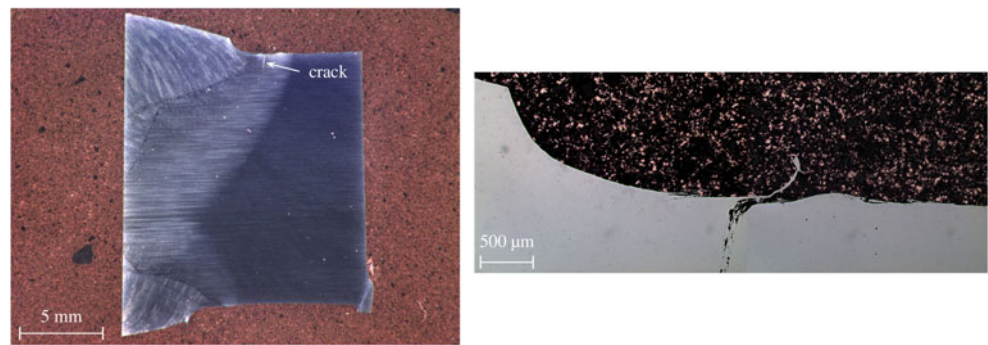
To study the influence of tool direction, butt weld assemblies made of S690QL steel grade have been retained. During the treatment (still realised on the semi-automatic installation), the angle of incidence of the indenters was set at 6° with respect to the normal at the assembly sheet.

In this case as well, a slight improvement is noted on the treated assemblies (red points and blue triangles on Fig. 11) compared with the results of the as-welded assemblies (black circles). The analysis of the fracture surface highlights that crack initiations are all located at the bottom of impact folds. Figure 12 reveals this phenomenon on a partially propagated crack from the non-broken side of a fatigue-loaded specimen.

These results tend to show that in the case of an angle of incidence close to base metal normal, the indenters first impact the weld toe from the side of the weld zone. Then they fold a part of metal under themselves, in the stress raiser zone, creating the folds observed.

¹ S355 equivalent steel grade dedicated to marine application.

Fig. 12 Microstructure of a S690QL butt-welded assembly treated by HFMI and detail of the crack initiation zone at the bottom of the groove



3 Modelling of the HFMI and the fatigue loading

3.1 Estimation of the local properties of the cruciform welded assembly required

3.1.1 Reverse method used

In the scope of the numerical modelling below, the case of the S355K2 cruciform joints selected previously is reused. The local mechanical characteristics of the assembly must be assessed in view of simulating high-frequency mechanical impact treatment. A suitable solution in the welding field results in taking microspecimens in the various assembly zones. Another solution involves using specimens with a simulated welding microstructure. However, these two solutions may be problematic and costly.

Over the last years, instrumented indentation (Fig. 13) has become an increasingly used analysis tool for characterising the local behaviour of materials. This technique is an interesting alternative for estimating the local properties of the various zones comprised in welded assembly, that is, the weld zone (that we will refer to as WZ), the heat-affected zone (HAZ) and finally the base metal. Chung et al. [13] therefore used spherical instrumented indentation coupled with a finite element analysis, using an inverse method, to assess the local mechanical behaviour of welded assemblies.

We selected a method defined as reverse for greater speed and simplicity of use. It is based on a set of numerical indentations which are post-treated in order to determine analytical relations between mechanical properties and indentation curves. These analytical relations can thus be used on many indentation curves without perform anymore modelling (unlike invert methods). The reverse method used in our case is based on the spherical type instrumented indentation and restricted to metallic materials whose mechanical behaviour may be considered of elastic–plastic type with linear kinematic hardening. Knowing the Young's modulus E and the Poisson's ratio ν , it helps to estimate two parameters,

the yield strength σ_y and the hardening modulus H as during a tensile test:

$$\text{In the elastic domain : } \sigma = E \cdot \varepsilon \quad (2)$$

$$\text{In the elastic–plastic domain : } \sigma = \sigma_y + H \cdot \varepsilon^p$$

$$= \frac{E}{E + H} (\sigma_y + H \cdot \varepsilon) \quad (3)$$

3.1.2 Application of instrumented indentation to the welded assembly

Firstly, three instrumented spherical indentations series were carried out through the three zones making up the studied fillet weld assembly. All the indentation curves, performed with the same indenter as that used by Collin et al. [14], are presented on the Fig. 14. The position of the cross-section of the tensile test specimen taken in the base metal is also included in this figure. The maximum load applied on the indenter was set to 200 N for the base metal and the weld zone. A lighter load² (100 N) was applied for the heat-affected zone in order to limit the size of the indented zone with respect to the more restricted width of the HAZ.

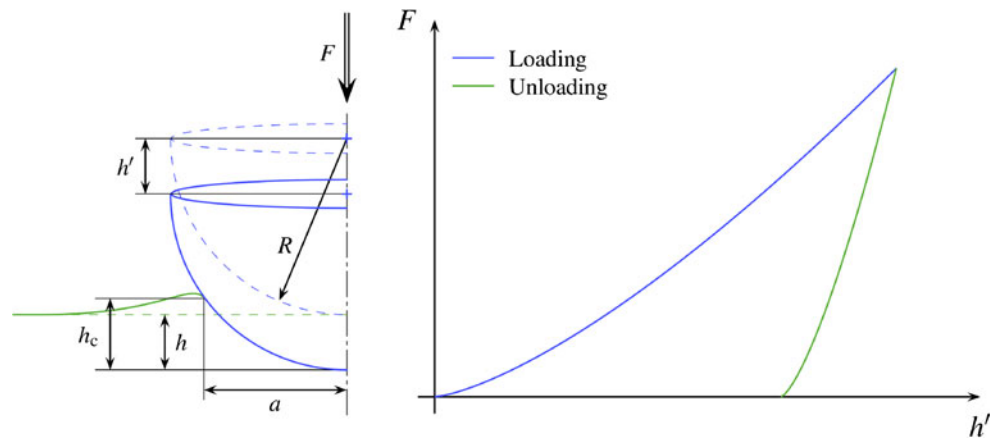
3.1.3 Estimation of the local tensile curves

Secondly, the reverse method [15] was applied in order to assess the local properties of the welded assembly from the indentation curve obtained. Figure 15 presents all the local properties estimated. A good concordance between the estimated results of the base metal and the related reference tensile curves is noted.

However, there is a significant difference observed between the tensile curve obtained on a weld metal specimen

² An excessively high load will result in an excessively large indented zone and consequently an averaged result over this zone, whereas an excessively low load results in a decrease in the measurement accuracy and repeatability. This notably depends on the grain size which may be relatively significant in a heat-affected zone.

Fig. 13 Schematic representation of a spherical indentation (left hand) and general shape of a conventional instrumented indentation curve (right hand)



taken from an ‘equivalent’ butt-welded assembly and the approximate curves by the reverse method of the cruciform assembly. An additional instrumented indentation was carried out in the centre of the weld zone of the butt-welded assembly. The corresponding estimated indentation curve is outlined in red on Fig. 15. This additional estimate is closer to the behaviour of this zone obtained by means of the tensile test. Given the difference in behaviour obtained between the weld zone of the butt-welded assembly and the weld zone of the cruciform

assembly, only the data estimated by instrumented indentation on the latter was selected for the rest of the study.

3.2 Modelling of high-frequency mechanical impact

3.2.1 Direct method dedicated to discontinuous mobile loading

We implemented and used a direct method dedicated to discontinuous mobile loadings [15] in order to model

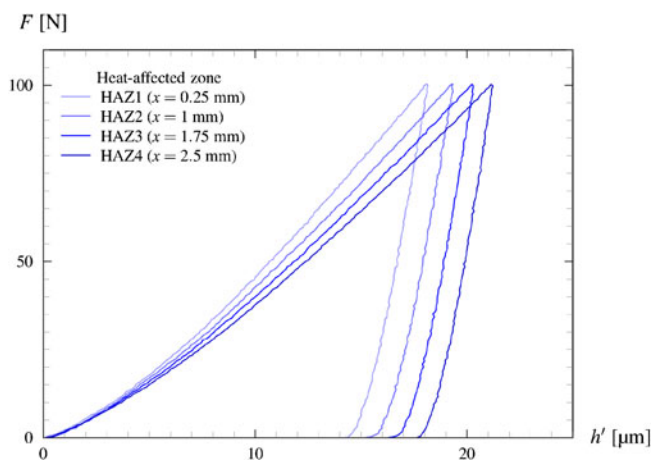
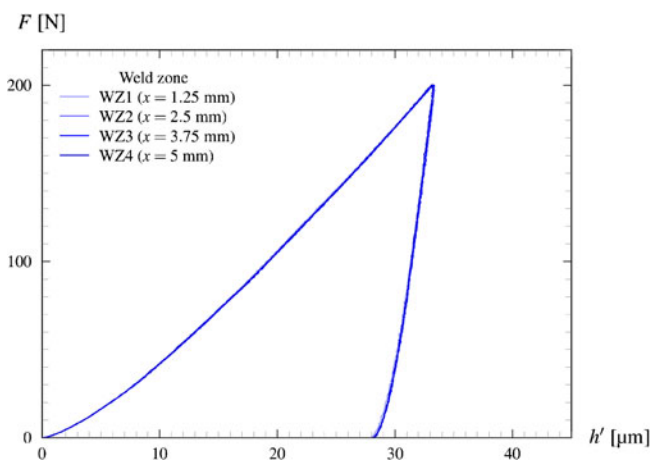
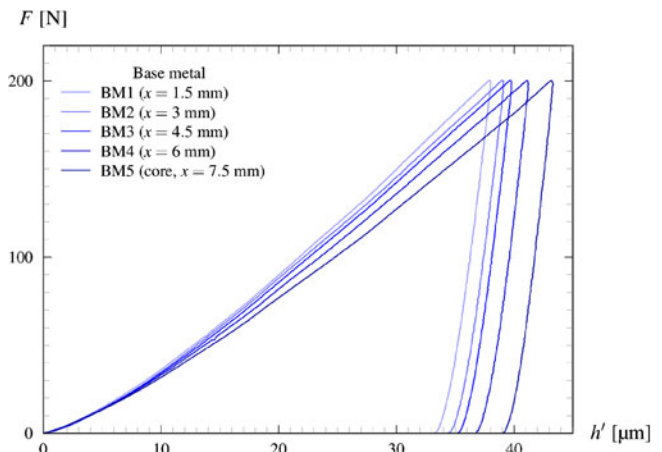
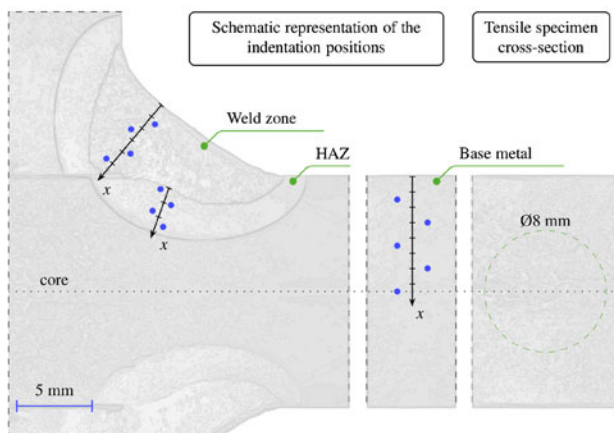


Fig. 14 Indentation sets through each zones of the fillet weld

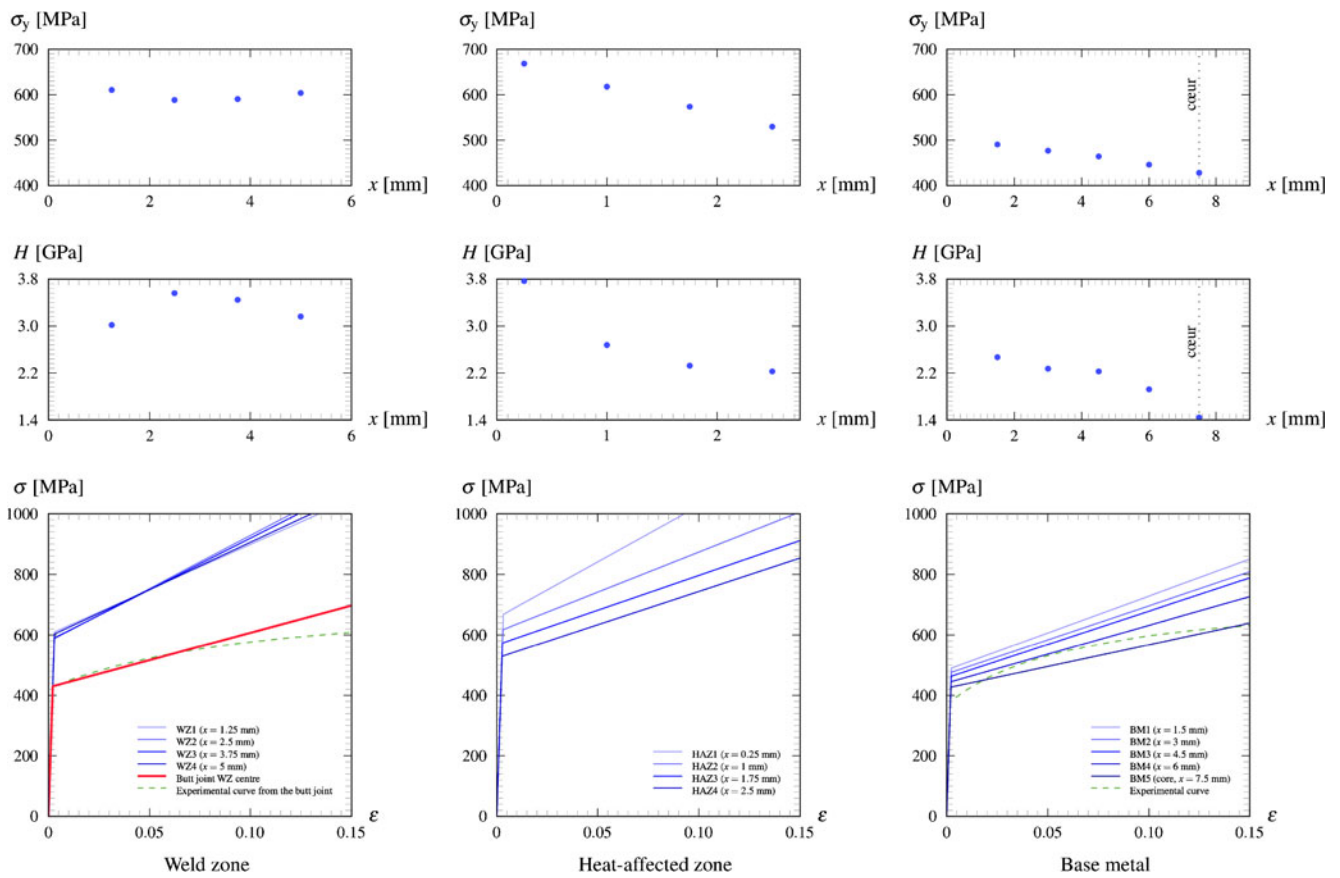


Fig. 15 Estimation of mechanical characteristics from instrumented indentation curves

treatment by high-frequency mechanical impact. This method which is based on finite elements, is an extended version of the pass-by-pass stationary method [16] and, subject to certain conditions, makes it possible to simulate the treatment in a much more limited time-frame than with the traditional incremental method (step-by-step) and with the same calculation accuracy.

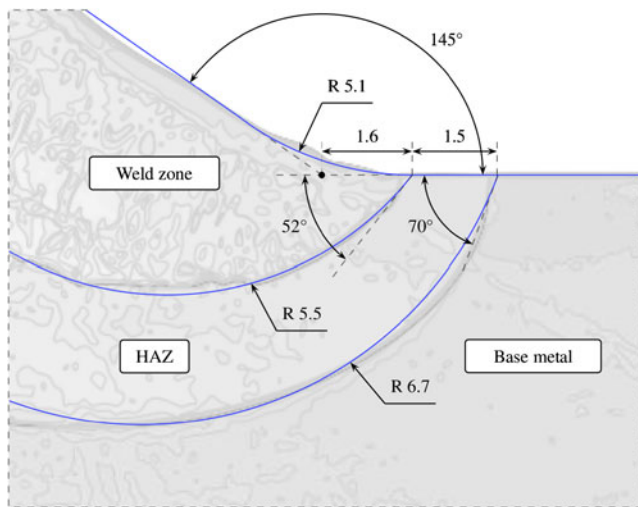


Fig. 16 Geometry and dimensions selected for the modelled weld toe

3.2.2 Weld toe configuration and indenter position

A simplified geometry was selected for modelling HFMI on one of the fillet welds of the cruciform welded assembly. The detail of the weld toe dimensions is provided in Fig. 16. Circular boundaries between the weld zone, the HAZ, and the base metal are shown in Fig. 17.

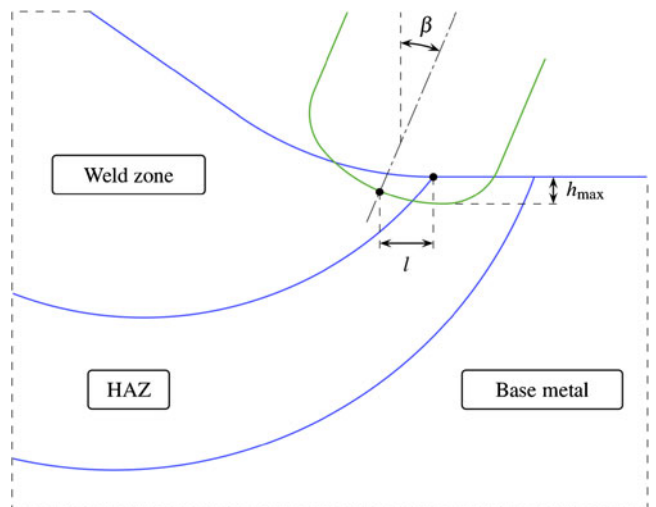


Fig. 17 Indenter location and direction parameters with respect to the weld toe

HAZ and the base metal were defined and will be used to assign the local mechanical properties of each of these 3 zones.

The parameters characterising the position and the direction of the indenter with respect to the simplified geometry of the weld toe are outlined on Fig. 17. Figure 17 also represents the indenter in its maximum sinking position, noted h_{max} . The additional parameters, β and l , respectively help to direct the indenter with respect to the vertical and to position it laterally with respect to the weld toe.

3.2.3 Presentation of the mesh and allocation of mechanical properties

The mesh of the welded assembly is composed of 2 main parts. One part loaded in the elastic domain, in blue on Fig. 18, and one elastic–plastic part, green, comprising the zone where a plastic flow may occur. This zone is divided into 12 identical segments. Their thickness has to correspond to the mean distance between impacts measured on our treated assemblies, that is approximately 60 μm . Thus, the frequency measured previously is indirectly taken into account. The direct method dedicated to discontinuous mobile loadings will only be applied on the elastic–plastic part of the mesh.

The elastic properties selected for the welded assembly are those of the base metal, that is:

- $E=205$ GPa and $\nu=0.3$.

The elastic–plastic zone is assumed to be of linear kinematic hardening. We proposed to simplify the development of the properties estimated by instrumentation indentation in order to make it easier to allocate these properties to the assembly mesh. The weld zone is assumed to be homogeneous, as well as the base metal by selecting the behaviour estimated around the surface. The continuity between these

two zones will be ensured by a linear distribution of the properties through the HAZ.

The yield strength of the weld zone (σ_{ywz}) and its hardening modulus (H_{wz}) will be set to:

- $\sigma_{ywz}=620$ MPa and $H_{wz}=3$ GPa.

Whereas those of the base metal will be set to:

- $\sigma_{ywz}=490$ MPa and $H_{wz}=2.4$ GPa.

Only the tip of an indenter is modelled (over a length of 5 mm). In the example dealt below, the indenter is directed with respect to the weld toe by reusing the angle of incidence used during actual treatment, that is $\beta=23^\circ$ (with respect to the vertical as illustrated in Fig. 18). Parameters l and h_{max} will be respectively set to 1.3 mm and 0.4 mm. Its mechanical behaviour is assumed to be elastic with a Young's modulus of 210 GPa and a Poisson's ratio of 0.3.

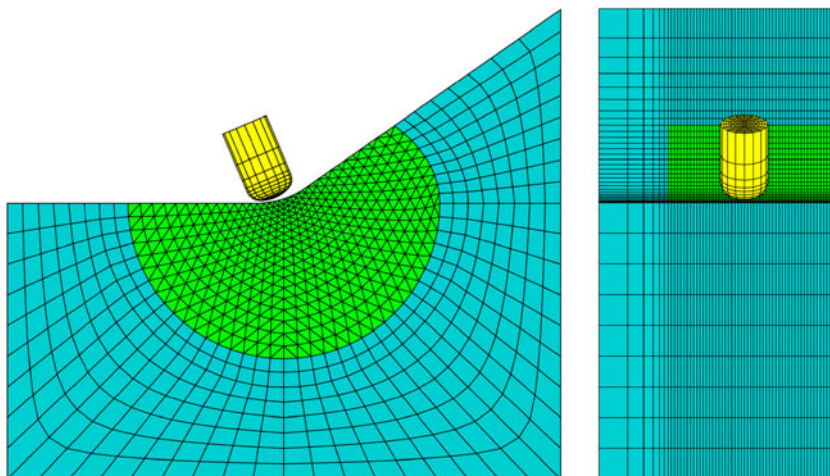
3.2.4 Simulation of HFMI treatment

During the simulation, frictions as well as the heating that may be caused by friction between the surfaces in contact and heat dissipations from plastic strain are not taken into account during mechanical impact simulations. It is also assumed that there are no initial residual stresses, even though in principle they may affect the state of stresses obtained after treatment. Finally, the loading applied to the structure is assumed to be quasi-static.

Indenter loading conditions:

- The upper part of the indenter is displacement-controlled in the direction given by its axisymmetric axis.
- The loading parameter corresponds to the vertical component h_{max} of controlled displacement from the indenter. Its 0.4 mm value ensures a groove depth after treatment equivalent to that observed during the experiments (ranging between 0.15 and 0.25 mm).

Fig. 18 Position and direction of the indenter at the weld toe



- The direct method dedicated to discontinuous mobile loadings is applied during loading on the assumed elastic–plastic part.
- Indenter unloading is ensured during a second step during which the direct method is not applied.

The distribution of estimated residual stresses for the set of parameters considered is illustrated in Fig. 19. Note that high compression residual stresses (approximately 550 MPa) are created at a depth of several millimetres. However, they are more moderate around the surface where the numerical value is about -50 MPa which is close to the previous experimental ones obtained by XRD in the same area (-80 MPa in average, Fig. 6).

Figure 20 presents the residual stress field, still in the transverse direction to the groove. Only a segment of the mesh (stemming from the assumed homogeneous zone downstream from the indenter) is represented.

3.3 Modelling of the fatigue loading

A direct method dedicated to cyclic loading [15], which was implemented in the software used, is applied to carry out the fatigue loading simulation. This simulation will only be applied on a segment taken in the homogeneous zone of the groove generated by the treatment. All the fields characterising its state after the mechanical impact simulation are considered as the initial state before cyclic loading is applied.

3.3.1 Cyclic loading simulation

The segment in Fig. 20 is used here. It is subject to fully reversed fatigue loading for a stress range set to 566 MPa (in terms of nominal stress). This loading corresponds to the highest level applied during the fatigue tests experiments. According to the results obtained, an elastic shakedown occurs in the zone around the groove. The new stress

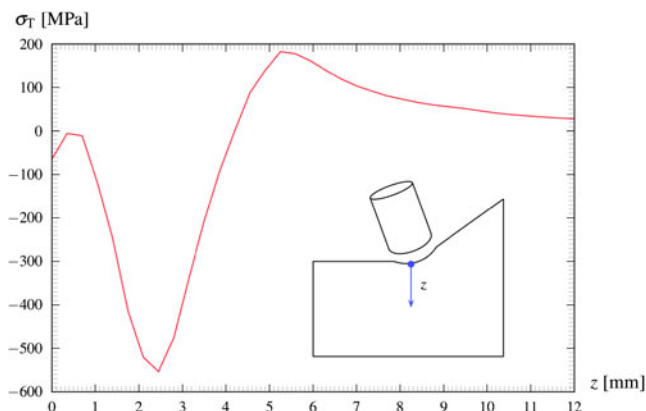


Fig. 19 Distribution of stresses in the transverse direction to the groove versus depth z , starting from the hollow of the groove

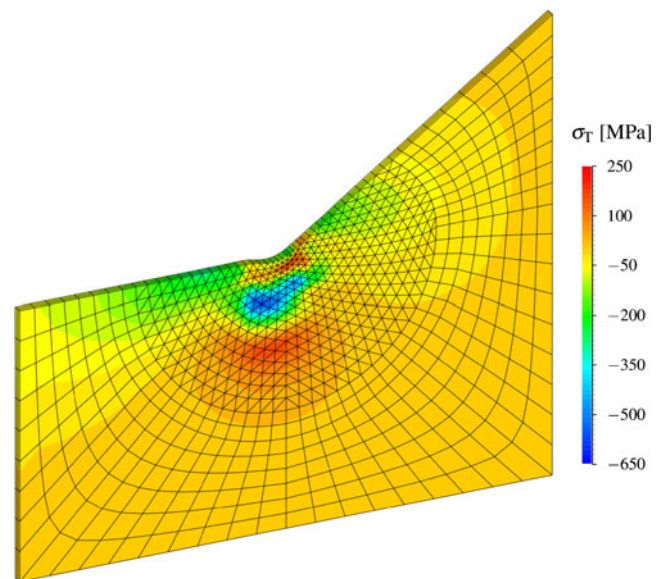


Fig. 20 Nodal interpolated field of residual stresses in the transverse direction to the groove on a segment taken from the homogeneous zone

distribution based on the depth starting from the hollow of the groove is given in Fig. 21 (in comparison with the reference distribution stemming from Fig. 19). A significant relaxation of the residual stresses can be noted in the zone with the higher values. Near the surface, residual stresses tend to remain constant, in accordance with the previous XRD measurement performed on a specimen after the same fatigue loading (Fig. 7). Their range at stabilised state remains potentially beneficial for better fatigue strength combined with the weld toe geometry, which is not altered by cyclic loading.

3.3.2 Analysis of the new fatigue life

In addition to the distribution of residual stresses presented in Fig. 21, the strain range is recovered versus the depth underneath the treated groove. Moreover, the Manson–Coffin–

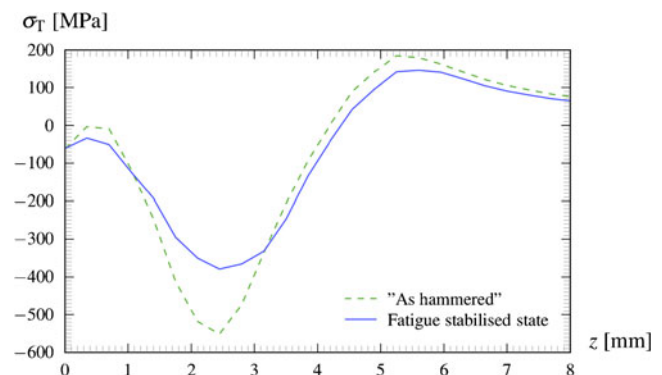
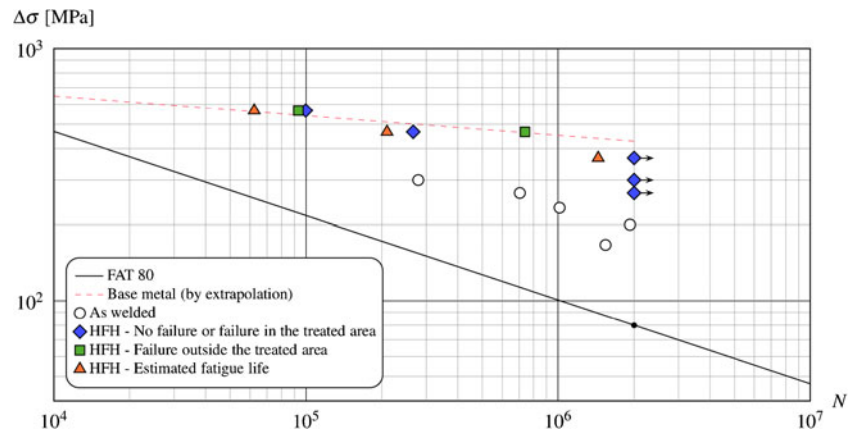


Fig. 21 Stress relaxation under the effect of fatigue loading ($\Delta\sigma=566$ MPa)

Fig. 22 Numerical estimation of the fatigue life of cruciform welded assemblies compared with experimental results (at $R=-1$)



Basquin relation [17–19] modified by Morrow [20] is considered, that is:

$$\frac{\Delta \varepsilon^t}{2} = \frac{\sigma'_f - \sigma_{moy}}{E} (2N)^b + \varepsilon'_f (2N)^c \quad (4)$$

Where $\Delta \varepsilon^t$ and σ_{moy} are respectively the local total strain range and the local mean stress, estimated numerically in the groove.

By using a binary search algorithm, we can therefore deduce the fatigue life N of the welded assembly. The local cyclic properties required are assumed to be similar to those of the base metal, estimated by low cycle fatigue tests with: $\sigma'_f = 70$ 2.5 MPa; $\varepsilon'_f = 27.2\%$; $b = -7.82 \cdot 10^{-2}$; $c = -5.51 \cdot 10^{-1}$. Note that equivalent results have been obtained by using directly the Uniform Material Law [21] as well as the medians method [22]. A procedure was implemented in the finite element calculation software used in order to directly estimate the distribution of N after calculation of the stabilised state.

The minimum obtained for fully reversed loading of 566 MPa correspond approximately to 10^5 cycles and is located on the HFMI groove surface. This can be explained by the residual compressive stresses which are more moderate around the surface in addition to the stress raiser

caused by the groove. As will be subsequently seen, this life is relatively close to that obtained experimentally for this high level of loading.

3.4 Fatigue lives estimated from the previous approach

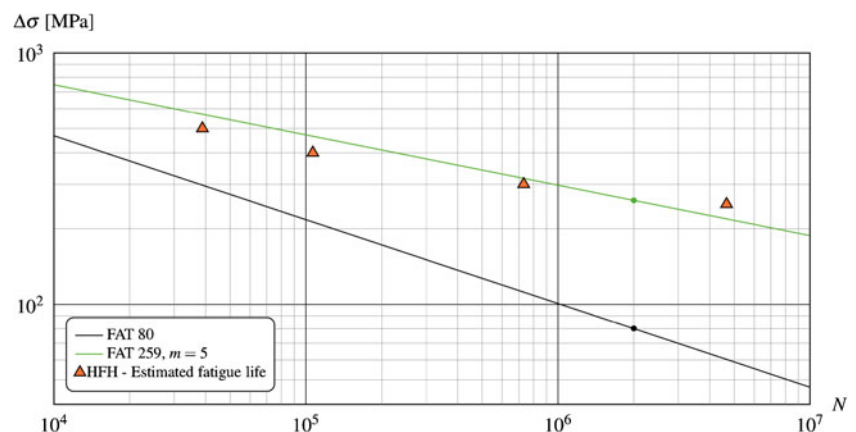
The fatigue lives related to various cyclic loading levels have been estimated and represented in Fig. 22 with those experimentally determined.

For a fully reversed fatigue loading ($R=-1$), the numerically estimated results are in accordance with those experimentally obtained, even though the selected fatigue life law is very simple. They are slightly underestimated which may partly be explained by the fact that the local hardening state is not taken into account in the fatigue life calculation. The cyclic properties considered are only those of the base metal.

The distribution of stresses and the fatigue life of the assembly were estimated again with a stress ratio corresponding in this case to $R=0.1$, for various loading levels. The obtained results were compared on Fig. 23 to the fatigue class (FAT) proposed by Pedersen et al. [23] for these loading conditions on this type of assembly.

Here again, there is a good agreement between the numerical results estimated by means of the approach proposed and the FAT class inferred from a compilation of the experimental

Fig. 23 Numerical estimation of the fatigue life of the cruciform welded assembly for a stress ratio corresponding to $R=-0.1$



results by Pedersen et al. [23]. However, it should be noted that the numerical results estimated correspond to a 50 % survival probability and a FAT class corresponds to the survival probability of 95 % at a confidence level of the mean of 75 %. Thus, the class FAT given by Pedersen et al. is not conservative compared to our results. The hardening state may once again partly explain the offset of our results which, however, places the estimated fatigue lives on the ‘security side’.

4 Conclusions

The aim of the study was first to better understand the effect of HFMI on the fatigue life improvement provided of steel welded assemblies. Secondly, a numerical approach has been developed in order to optimising the HFMI process while taking into account the operating parameters, the impacted materials and the quality of the weld.

The following points are worthy to be noted concerning the experimental part:

- With optimised HFMI treatment conditions, the results obtained are well in line with those of the literature;
- Even though the welded assemblies have good behaviour in the as-welded state, a significant improvement in fatigue strength was noted after treatment;
- The residual compressive stresses measured in the groove created by HFMI are relatively low in the loading direction;
- The improvement of the local geometry and moving the initiation point with respect to the initial weld toe are significant parameters;
- The reduced number of indenters (two instead of four normally used) does not seem to have affected these results;
- The estimated impact frequency is markedly lower than those indicated in literature;
- The results presented on several assembly batches seem to highlight the importance, on the one hand, of the initial weld toe geometry and, on the other hand, the conditions of use of the tool (direction, pressure, etc.) in relation to the risk of impact folds appearing.

All of these observations reveal the importance of developing a consistent and robust approach with the aim of defining the optimum operating conditions of the process. The numerical approach developed in this study leads to calculated fatigue lives which are in keeping with those from the experimental tests. Therefore, the obtained numerical results make it possible to consider developing software either to estimate the fatigue life of a treated structure or to optimise the treatment parameters of high-frequency mechanical impact.

References

1. Haagenen PJ, Maddox SJ (2007) IIW recommendations on post weld improvement of steel and aluminium structures, International Institute of Welding (XIII-2200-07)
2. Maddox SJ (2003) Key developments in the fatigue design of welded constructions. *Weld World* 47:7–40
3. Statnikov ES, Trufyakov VI, Mikheev PP, Kudryavtsev YF (1996) Specification for weld toe improvement by ultrasonic impact treatment, International Institute of Welding (XIII-1617-96)
4. Lihavainen VM, Marquis G (2006) Fatigue life estimation of ultrasonic impact treated welds using a local strain approach. *Steel Res Int* 77:896–900
5. Roy S, Fisher JW (2005) Enhancing fatigue strength by ultrasonic impact treatment. *Int J Steel Struct* 5:241–252
6. Nitschke-Pagel T, Dilger K, Eslami H, Weich I, Ummerhofer T (2007) Residual stresses and near surface material condition of welded high strength steels after high frequency mechanical post-weld treatments, International Institute of Welding (XIII-2153-07)
7. Marquis G (2010) Failure modes and fatigue strength of improved HSS welds. *Eng Fract Mech* 77:2051–2062
8. Yildirim HC, Marquis GB (2012) Overview of fatigue data for high frequency mechanical impact treated welded joints. *Weld World* 57(7/8), in print
9. Statnikov ES, Vityazev V, Korolkov O (2004) Comparison of the efficiency of 27, 36 and 44 kHz UIT tools, International Institute of Welding (XIII-2005-04)
10. Statnikov ES, Korostel VY, Vekshin N, Marquis G (2006) Development of esonix impact treatment techniques. International Institute of Welding (XIII-2098-06)
11. Bousseau M (2010) Post-treatment by UIT process of a cruciform welded joint made of DH36 steel grade (Parachèvement par le procédé UIT d’un joint soudé en croix en acier DH36), DCNS (CESMAN)
12. Bousseau M (2010) Post-treatment by UIT process of a butt-welded joint made of S690QL steel grade (Parachèvement par le procédé UIT de joints soudés bout à bout en acier S690QL), DCNS (CESMAN)
13. Chung K-H, Lee W, Kim JH, Kim C, Park SH, Kwon D, Chung K (2009) Characterization of mechanical properties by indentation tests and FE analysis—validation by application to a weld zone of DP590 steel. *Int J Solids Struct* 46:344–363
14. Collin J-M, Mauvoisin G, Pilvin P, El Abdi R (2008) Use of spherical indentation data changes to materials characterization based on a new multiple cyclic loading protocol. *Mater Sci Eng* 488:608–622
15. Le Quilliec G (2011) Application of high frequency hammer peening for the maintenance optimisation of civil engineering equipments and welded structures (Application du martelage à haute fréquence à l’optimisation de la maintenance des ouvrages et des structures soudées), PhD Thesis, École Centrale de Nantes-École Doctorale Sciences Pour l’Ingénieur Géosciences Architecture
16. Dang Van K, Maitournam MH (1993) Steady-state flow in classical elastoplasticity: application to repeated rolling and sliding contact. *J Mech Phys Solids* 41:1691–1710
17. Manson SS (1952) Behavior of materials under conditions of thermal stress, heat transfer symposium. University Michigan Press, Ann Arbor
18. Coffin LF (1954) A study of the effects of cyclic thermal stresses on a ductile metal. *Trans of ASME* 76:931–950
19. Basquin OH (1910) The exponential law of endurance tests, proceedings of the ASTM 10, American Society for Testing and Materials 625–630

20. Morrow J (1965) cyclic plastic strain energy and fatigue of metals, internal friction, damping and. Cyclic Plasticity, ASTM STP 378, American Society for Testing and Materials, 1965 45–87
21. Bäuml AJ Seeger T (1990) Materials data for cyclic loading—supplement I. Elsevier Science, Amsterdam
22. Meggiolaro MA, Castro JTP (2004) Statistical evaluation of strain-life fatigue crack initiation predictions. *Int J Fatigue* 26:463–476
23. Pedersen MM, Mouritsen O, Hansen MR, Andersen JG, Wenderby J (2010) Comparison of post weld treatment of high strength steel. *Weld Joints Medium Cycle Fatigue*, 54(7/8)